A Photonics-Assisted Multi-Band MIMO Radar Network for the Port of the Future

Giovanni Serafino, Salvatore Maresca, Luca Di Mauro, Alexandr Tardo, Antonio Cuillo, Filippo Scotti, Paolo Ghelfi, Paolo Pagano, Antonella Bogoni

***Abstract*— The Internet-of-Things paradigm is pushing the current fully-automated industry to Industry 4.0, laying on a high degree of end-to-end digitization of all physical assets and their integration into data-based services. A significant contribution to recent advances of digital technologies comes from microwave photonics, whose benefits for RF systems in terms of performance and flexibility have been largely demonstrated. In the radar domain, the high degree of coherence granted by photonics makes possible multiple input-multiple output systems, enabling an enhancement of surveillance and monitoring capabilities, thanks to the possibility of performing centralized processing and raw-data fusion. The advantages offered by photonics for surveillance converge with the Industry 4.0 revolution, helping in the actualization of the "Port of the Future" paradigm, to monitor the freight traffic inside ports, increasing goods distribution efficiency, at the same time reducing carbon footprint. Here, we present the first photonics-based widely distributed multiple input-multiple output dual-band radar network, designed to operate in a real port, showing the achieved enhanced potential detection and imaging capabilities. The integration of the targets radar tracks within the monitoring and control platform of the port is reported, enabling the fusion with other data managed by the multiservice monitoring platform.**

***Index Terms*— Microwave Phonics, MIMO Radar, Surveillance, Industry 4.0**

I. Introduction

THIS new millennium is witnessing the dawn of the so-called fourth industrial revolution, triggered by the impressive recent advances of novel technologies related to information and communications, which are converging with industrial manufacturing and management processes. In the framework of Industry 4.0 [1], a key role is played by trading hubs like ports, since a huge amount of the freight traffic is hauled on sea routes. Until 2019, maritime trade knew an average growth of 3.5% per year. Then, it started slowing down due to lingering trade tensions, with a remarkable turnaround caused by the CoViD-19 pandemic [2]. However, it is a common opinion that the present situation is temporary, and that the next future will lead back to growing trends that will intensify the ship traffic around the world and inside the ports. Therefore, ports management keeps on being crucial for productivity and distribution and, for this reason, many port authorities are adopting the Smart Port, or Port of the Future paradigm [3], driven by novel technologies. Pervasive sensing and machine-to-machine (M2M) communications, mainly based on the newly available 5G infrastructures, find new applications to increase the efficiency in all the processes related to production and distribution of goods, aiming at a continuous, though sustainable, economic growth [4].

Generally, major maritime carriers are demanding improvements in the efficiency of port operations. Cargo carried by ships must be loaded and unloaded quickly with minimal stopover time in the port. This is driving the implementation of more efficient processes and the reorganization of technologies in the terminals: connected platforms, cloud-based services, service-oriented architectures, sensors and other Internet of Things (IoT) technologies, like M2M, augmented reality (AR), autonomous transportation, next generation 5G mobile networks, and blockchain-based technology. In order to respond to Smart Port/Port of the Future requirements, an approach based on the usage of monolithic technological solutions has been avoided, to the advantage of system scalability.

In this picture, photonics is more and more recognized as a key enabling technology that can drive the development of new sensing solutions for surveillance and traffic monitoring. In particular, benefits come from microwave photonics (MWP) [5], [6], which is the branch of photonics employed for the generation, processing, and acquisition of RF signals. This technology is nowadays entering the age of maturity, thanks to the advances in the realization of photonic devices, and to the impressive leaps forward made by photonic integrated technology [7], which made MWP systems more rugged and reliable. Nowadays, MWP enables the adoption of novel

This paragraph of the first footnote will contain the date on which you submitted your paper for review. It will also contain support information, including sponsor and financial support acknowledgment.

This work was supported in part by the projects NATO SPS SOLE (G5267), H2020 COREALIS (#768994), H2020 ROBORDER (#740593), and iNGENIOUS (#957216).

G. Serafino, S. Maresca, L. Di Mauro, and A. Bogoni are with Sant'Anna School of Advanced Studies, via G. Moruzzi 1, Pisa, 56124, Italy (corresponding author e-mail: g.serafino@santannapisa.it).

A. Cuillo, A. Tardo, F. Scotti, P. Ghelfi, and P. Pagano are with Consorzio Nazionale Interuniversitario per le Telecomunicazioni (CNIT), via G. Moruzzi 1, Pisa, 56124, Italy.

approaches for the implementation of pervasive, flexible sensor networks [8]-[10], which can be integrated with wider surveillance platforms that help monitoring and managing the port traffic. Indeed, MWP allows for the deployment of centralized multiple input-multiple output (MIMO) radar systems composed by widely separated antennas which, up to now, have been hardly feasible with traditional RF technology. Photonics-based monostatic radars for a maritime environment [11], as well as MIMO radar solutions have been recently proposed [8], [9] and demonstrated in laboratory [12] as well as in outdoor multi-target simple scenarios [13]. The design approach and system functionalities have been validated [14], demonstrating the capability of photonics-assisted multi-band coherent MIMO radar systems to grant enhanced detection and localization performance with respect to single-band stand-alone systems.

Photonics grants an unprecedented flexibility to radar systems, enabling them to transmit and receive signals from different sites, but also to simultaneously handle different waveforms on different RF carriers. Photonics-assisted generation, distribution, and reception of RF signals [9], [15], [16] bring about the major benefits of an inherent high signal stability and phase synchronization among the MIMO radar network peripherals. This, in turn, allows for a coherent fusion of the information collected by many peripherals at a raw data level, which translates in enhanced resolution and imaging capabilities [14]. Therefore, a widely distributed radar network not only offers typical advantages of radars, like day-and-night, all-weather surveillance, but also improved performance, enabling better target classification and identification. The consequent increased situational awareness, beyond the possibility of avoiding in-port disastrous accidents occurred in the past [17], can be employed for traffic management of ships inside or approaching the port. In addition, the increased system capability of detecting even small boats can be employed to spot malicious intruders in ports with sensitive structures, like oil docks. Finally, the MIMO system output can be merged with the outputs from other sensors already exploited for port surveillance, e.g., cameras and lidars. Hence, processing approaches for fusing data from the MIMO radar with other heterogeneous sources are to be sought, to achieve the most accurate picture of the monitored scene.

Stepping from down-scaled and proof of concept experiments [13], [14], here we report the advances in the development of a photonics-assisted, multiband MIMO radar network, whose deployment for surveillance in a real freight port is underway at the Livorno Port, Italy, one of the major freight ports in the European Union (EU). For the system to be suitable for deployment in a real harbor, its design must address the specific mission requirements. In this paper, *ad-hoc* modeling and data fusion algorithms have been exploited for simulating the whole system operation, considering a common port multi-target scenario, dealing with the design complexity due to the large number of parameters to be optimized, from the network topology to the employed waveforms, the hardware requirements, the specific processing algorithms, and so on. However, a trade-off between performance and complexity and cost has been pursued, aiming at minimizing the number of employed radar network nodes and operating bands.

Moreover, the integration of the MIMO radar functionality with the existing port multiservice control platform (monitoring control application, Moni.C.A.) is reported. An example of the interaction between the Moni.C.A. standard platform [18] and the MIMO radar is shown, stepping from a real Automatic identification system (AIS)-recorded track. The association to the target tracks of the information collected by the radar demonstrates the enhanced control of the port area, thanks to the possibility of fusing information generated by heterogeneous sensors.

II. Photonics-Enabled MIMO Radar Networks

Distributed, multi-site radars represent a breakthrough overcoming the traditional concept of stand-alone, local radar, introducing the concept of network in the radar world [19]. Distributed systems, in which each node can receive the echoes coming from signals transmitted by other nodes in the network, has become famous under the name of MIMO radars [20], for its similarities with MIMO communication systems.

A. Multisite, Multiband Systems with Centralized Processing

A major advantage offered by MIMO radars is the increase of the spatial resolution [20], [21] compared to stand-alone radar systems, both in range and cross-range directions. In monostatic radars, the range resolution is determined by the bandwidth of the transmitted signal, the cross-range resolution depends on the antenna beam aperture and the target distance. Conversely, MIMO radars exploit spatially distributed information to achieve a better resolution both in range and cross-range [22]. Moreover, stand-alone radars can directly measure only the radial component of the target velocity vector from the Doppler frequency shift. MIMO radar systems, on the other hand, can measure both the components [23], with the possibility of an accurate reconstruction of the target trajectory and kinematics, allowing also precise target tracking.

The enormous potential of multi-site radars stands in their capability to exploit spatial diversity, by observing the same scene from different viewpoints, with benefits when detecting low-detectable targets, which are characterized by a small radar cross-section (RCS), or high angular RCS variability (e.g., stealth, or complex targets), or targets obscured by other radar echoes. Additional diversity can be obtained thanks to multi-band operation. Indeed, radars working in different spectral regions may increase the system detection capability and reliability, along with its robustness to the environmental conditions. Data fusion among multi-band and multi-site detections permits to exploit all the acquired information, increasing the system precision.

A multisite radar network can be implemented with a *decentralized* or *centralized* processing architecture. Multisite radars with *decentralized* processing consist of independent nodes, or radar peripherals (RPs), as in Fig. 1 a): each one observes the same scene from different viewpoints, transmits the radar waveforms and receives the back-scattered echoes from the targets, performing a first data processing locally on

This article has been accepted for publication in IEEE Journal of Selected Topics in Quantum Electronics. This is the author's version which has not been fully edited and content may change prior to final publication. Citation information: DOI 10.1109/JSTQE.2021.3092880

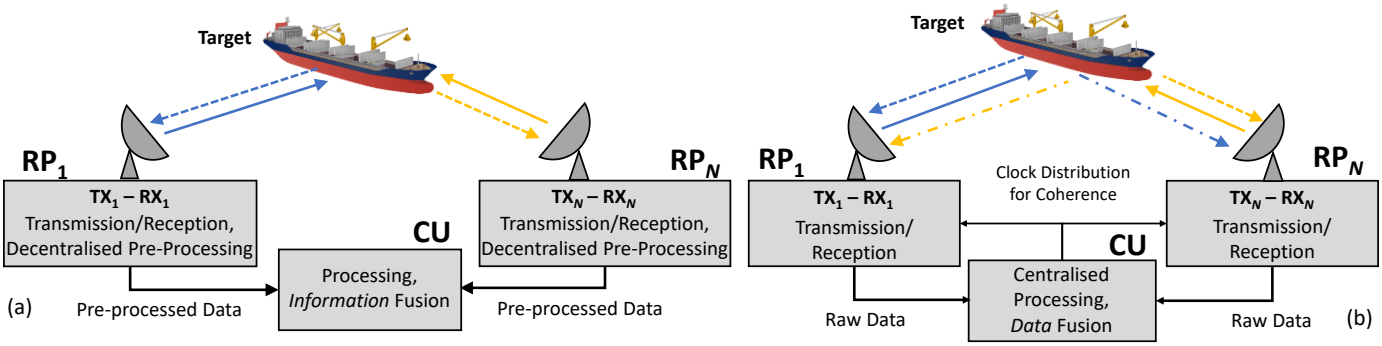

Fig. 1. Schematic of multisite radar systems exploiting two different approaches: decentralized (a) and centralized (b) processing. In the first case, each radar peripheral (RP) transmits its own generated waveform and receives only the echo of the waveform it transmitted, pre-processing the data before sending it to the central unit (CU) that performs information fusion; no coherence exists among the RPs, unless reconstructed by heavy post-processing. In the second case, RPs coherence is ensured by the common clock reference generated in the CU, which receives the gathered raw data and can perform a joint processing by fusing them.

the received signals. The information extracted by each RP is collected by a central unit (CU) that operates a fusion. Thus, a certain amount of information is inevitably lost, potentially reducing the system performance. On the other hand, a *centralized* processing can be implemented if the RPs send their raw data to the CU, as represented in Fig. 1 b), thus largely reducing the information loss. Distributed systems with centralized processing fully realize the MIMO radar paradigm, collecting complete information on the scene under observation, thus being able to precisely detect, recognize and classify different targets.

The centralized architecture provides better performance, but it requires, among the radar signals transmitted by the nodes, a certain level of coherence, guaranteed by a common time reference that can be distributed by the CU, as in Fig. 1 b). Here, "coherence" has a twofold meaning: *(i)* it refers to the long-time coherence of the employed RF signals, granted by high phase stability; *(ii)* from the networking point of view, it indicates the time/phase alignment between the CU and the RPs, better if it is obtained avoiding complex synchronization mechanisms. Furthermore, centralized processing can be coherent or noncoherent, depending on the applied algorithms. In the latter, a better resolution, localization accuracy, and target parameters estimation is possible. A MIMO system *does not* perform all the time coherent processing on the entire area under observation, since this can be too expensive in terms of time and computational resources. On the other hand, it can continuously operate non-coherent processing and, when a target is detected, the system starts performing coherent processing in a limited space around the detection region. This flexible approach allows maximizing the system performance where and when it is really needed, optimizing the usage of system resources.

B. *Operational Multistatic and MIMO Radars*

Although distributed MIMO radars, and multistatic radars more in general, have been deeply investigated from a theoretical point of view since almost twenty years ago, today many are the obstacles that still hinder the realization of real operational systems. Nowadays, multistatic radars do exist [24], [25], but only with decentralized processing. The implementation of fully centralized processing is still inadequate in terms of performance, due to the lack of extremely precise time synchronization and high phase coherence between all the RPs of the distributed system [26]. Moreover, the needed high-capacity links connecting RPs and CU must also maintain the signals coherence. Finding an RF solution to these problems is challenging, especially for largely distributed systems. In these cases, the coherence among data is usually reconstructed digitally through heavy synchronization algorithms with high computational complexity. Conversely, an approach based on photonics for signal generation and distribution can guarantee the needed level of coherence, as demonstrated in many works, such as [6], [8], [10], [12], [13], [14], [16].

The major design challenges include the necessity for a reliable and, possibly, reconfigurable data communications network, for timing synchronization and for significant computational complexity and power (e.g., for system control and signal processing). In addition to these, highly accurate location information must be available for every remote radar peripheral. Finally, in coherent systems, a highly accurate method of distributed oscillator frequency and phase control is also necessary. For these very reasons, at the best of the Author's knowledge, rare are the cases of active multistatic or MIMO radar systems based on RF technology which have been tested in real maritime surveillance environments. Among these, the NetRAD system [27] and its successor NeXtRAD [28], have allowed to collect over the past years a significant database of multistatic measurements of targets and clutter for research purposes.

NetRAD was originally designed as a low-cost commercial off-the-shelf (COTS) radar system, for operation in the S-band, whereas NeXtRAD has been designed for operation in the X and L frequency bands, up to 5 km distances. Its RPs are controlled by laptops connected to local network switches, and communications is done via WiFi links (at 2.4 or 5 GHz), which are limited by line-of-sight coverage. Every RP has its own mixer for frequency downconversion and ADC for a local pre-processing of the signals, as well as a memory unit for locally saving digitized data. Then, the RPs send pre-processed data to the CU on a WiFi link, with the possibility of sending also the raw digitized data for fusion. However, this approach does not implement a truly centralized processing since, unlike the

photonics-assisted system, pre-digitized or pre-processed data, instead of analog waveforms, are sent to the CU. This requires an accurate reconstruction of the network synchronization. To this aim, the peripherals are synchronized, triggered, and phased-locked by using GPS Disciplined Oscillators (GPSDO). Each RP is equipped with its own sample clock, driven by the GPSDO. For completeness, the NeXtRAD architecture and main parameters are summarized in [28] and [25].

Instead, more widespread is the use of passive radars in multistatic radar systems for maritime surveillance. An example of such technology, which has reached a good technical maturity level, is described in [29], where an alternative use of global navigation satellite system (GNSS) signals is considered. GNSS satellites offer a global coverage, thus potentially enabling continuous monitoring of both coastal and open sea areas, where this latter is the bottleneck of those passive radars based on terrestrial illuminators, such as active vessel traffic system (VTS) and passive digital video broadcasting-terrestrial (DVB-T) systems. Here, the multistatic configuration, with the addition of long integration times, is necessary to enhance the system sensitivity.

Thus, from an operational perspective, most of the netted radar systems today are passive, or monostatic systems which perform little, or no exchange of information with other systems monitoring a common surveillance region. However, the necessity of networked radars is just one of the aspects of a more complex vision of the future operational needs, where the increased complexity is driving for more sophisticated sensors which could allow for higher flexibility and agility, as well as for multi-mode/multi-functional RF capabilities over very large frequency ranges and with potentially huge bandwidth. Only recently, GaN has proven to be the most capable semiconductor technology to cope with such bandwidths and RF-output power requirements [30].

C. *The MIMO Radar Signal Model and Target Modeling*

In general, a MIMO radar system employs M TX and N RX radar front-ends. The real disposition of the presented photonics-based MIMO radar system is sketched in Fig. 2. The implemented architecture is composed by 3 transmit (TX)/receive (RX) nodes, the RPs, transmitting in two bands, connected to a CU. Therefore, in the presented case, $M = N = 3$. The monitored area can be modeled as a 3D Cartesian observation space, in which the generic triplet (x, y, z) denotes the East, North and Up (ENU) local coordinates of a point referred to the origin, fixed on the position of RP_1.

We denote the front-ends with TX_m and RX_n, being $m = 1, \dots, M$ and $n = 1, \dots, N$. Let us assume that the antennas illuminate K point scatterers P_k, with $k = 1, \dots, K$ belonging to one or more targets in the surveyed space. Moreover, since MWP allows for software-defined coherent multi-band operation, as demonstrated in [31], the CU can arbitrarily generate up to $L = 2$ different waveforms at L different carriers to be transmitted by TX_m. Thus, being $s_{m,l}(t)$ the low-pass equivalent of the l^{th} signal transmitted by TX_m, with $l = 1, \dots, L$, the signal received by RX_n can be written as [20]:

Fig. 2. Topology of the MIMO radar network in a real port for traffic monitoring. The system central unit (CU) is connected to the radar peripherals (RPs) with optical fiber (represented by yellow lines). The yellow-shadowed areas schematically depict the transmission pattern of the employed antennas.

$$r_{m,n,l}(t) = \sum_{k=1}^{K} a_{m,n,l}^{(k)} s_{m,l}\left(t - \tau_{m,n}^{(k)}\right) e^{j\varphi_{m,n,l}(t)} + c_{m,n,l}(t) + w_{n,l}(t), \quad (1)$$

with $a_{m,n,l}^{(k)}$ and $\tau_{m,n}^{(k)}$ denoting respectively the complex amplitude and the delay, and $\varphi_{m,n,l}(t)$ accounting for the overall phase shift introduced by the system architecture. This drift is mainly caused by the optical maser oscillator instability, as discussed in [6], and by the optical link [12], [15].

In eq. (1), the term $w_{n,l}(t)$ represents the normalized thermal noise of the system and it is modelled as additive white Gaussian noise (AWGN) with unitary power. The term $c_{n,l}(t)$ represents the sea clutter contribution, which is modelled as a AWGN process with power described according to the sea-state depending model proposed by [32]. Finally, $a_{m,n,l}^{(k)}$ and $\tau_{m,n}^{(k)}$ depend on the bistatic geometry among TX_m, RX_n and P_k:

$$a_{m,n,l}^{(k)} = \sqrt{\frac{P_{TX}^{(m,l)} G_{TX}^{(m,l)} A_{n,l} \sigma_{m,n,l}^{(k)}}{(4\pi)^3 k_B B_{n,l} T_n L_n \boldsymbol{d}^2(TX_m, P_k) \boldsymbol{d}^2(P_k, RX_n)}}, \quad (2)$$

$$\tau_{m,n}^{(k)} = \frac{1}{c}[\boldsymbol{d}(TX_m, P_k) + \boldsymbol{d}(P_k, RX_n)]. \quad (3)$$

Here, $P_{TX}^{(m,l)}$ and $G_{TX}^{(m,l)}$ are respectively the transmitted power and antenna gain at TX_m for the l^{th} waveform, $A_{n,l}$ is the effective area of the RX_n antenna for the l^{th} RF carrier $f_{RF}^{(l)}$, $\sigma_{m,n,l}^{(k)}$ is the bistatic RCS of scatterer P_k observed by TX_m and RX_n, k_B is the Boltzmann's constant, c is the speed of light, $B_{n,l}$ is the noise bandwidth, T_n and L_n are the noise temperature and the loss factor at RX_n. Finally, $\boldsymbol{d}(A, \mathrm{B})$ is the Euclidean distance between points A and B.

To model the radar echoes scattered from extended maritime targets, let us generalize the methodology described in [33]. Once the gridded area to be monitored is defined, the pixels which are candidate to become point-like scatterers are selected from the grid points falling inside the vessel contours.

However, to model in an intuitive, yet realistic, way the scattering contributions of different vessel structures, these are approximated as 2D Gaussian surfaces. Thus, each pixel

This article has been accepted for publication in IEEE Journal of Selected Topics in Quantum Electronics. This is the author's version which has not been fully edited and content may change prior to final publication. Citation information: DOI 10.1109/JSTQE.2021.3092880

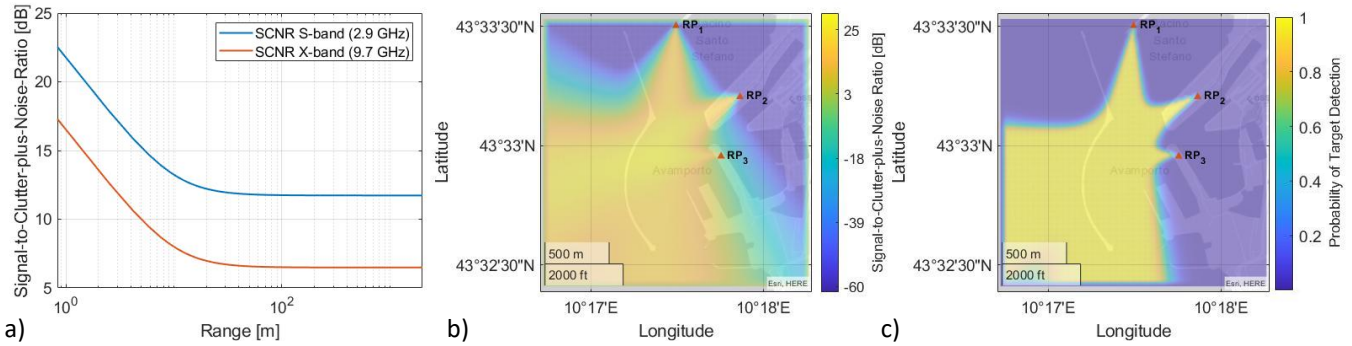

Fig. 3. Radar system sensitivity analysis considering a sea state of 5 on the Beaufort scale: a) SCNR evaluated for a monostatic radar operated in the S-band (blue line) and in the X-band (red line); b) SCNR evaluated for the proposed dual-band 3x3 MIMO radar system, deployed as in Fig. 2; c) Probability of detection evaluated from the estimated SCNR, considering a probability of false alarm of 10^{-4}. The CA-CFAR detection methodology proposed in [34] has been considered.

contributes to the overall target RCS according to its proximity to the most relevant structures (e.g., bow, stern, bridge, mainmast, tower cranes). This proximity permits to evaluate the corresponding percentage of the scatterer form the average target RCS, which can be retrieved for the different vessel types from the formula reported in [32].

D. The MIMO Radar Ambiguity Function

The proposed system architecture allows performing centralized processing at the CU, where the signals collected from all the RPs are gathered and combined within the DSP block. The target position can be determined from the maximum of the log-likelihood function of the target location $\vec{X}$ evaluated from all the virtual channels. The total number of virtual channels is $M \times N \times L$.

As described in [20], it is possible to calculate the MIMO ambiguity function (AF) $A(\vec{X})$ for non-coherent processing as:

$$A_{NC}(\vec{X}) \triangleq \frac{1}{(MNL)^2}\left|\sum_{m=1}^{M}\sum_{n=1}^{N}\sum_{l=1}^{L}\Psi_{m,n,l}(t,\tau_{m,n})\right|^2, \quad (4)$$

where $\Psi_{m,n,l}(t,\tau_{m,n})$ represents the cross-correlation between $r_{m,n,l}(t)$ and $s_{m,l}(t)$.To obtain an overall picture of the monitored area, the ambiguity function in eq. (4) is evaluated for each point $\vec{X}$ in the observation space.

Instead, for coherent processing [20]:

$$A_C(\vec{X}) \triangleq \frac{1}{(MNL)^2}\left|\sum_{m=1}^{M}\sum_{n=1}^{N}\sum_{l=1}^{L}E_l(\tau_{m,n})\cdot\Psi_{m,n,l}(t,\tau_{m,n})\right|^2 \quad (5)$$

where:

$$E_l(\tau_{m,n}) \triangleq e^{-j2\pi f_{RF}^{(l)}\tau_{m,n}} \quad (6)$$

are exponential terms which depend on the l^{th} RF carrier f_{RF} and on the underlying bistatic geometry among TX_m, RX_n, and the generic point $\vec{X}$. After this phase compensation, as described by eq. (5), the complex correlation contributions can be summed together coherently.

E. Exploiting MIMO Radar Data for Maritime Surveillance

To provide the operator with a clear maritime picture of the surveilled area, it is necessary to process MIMO radar data (i.e., non-coherent and coherent ambiguity functions) for evaluating how many targets are present in the area (i.e., target detection), for modeling their dynamic behavior (i.e., target tracking), and for possibly estimating their size (i.e., target classification).

Target detection is performed by associating to a set of cells under test (CUTs) a threshold, based on the received signals statistics, dimensioned to keep the false alarm rate below a pre-defined level. These detectors are said to have the constant false alarm rate (CFAR) property [34]. In this work, the cell averaging CFAR (CA-CFAR) detection strategy which is employed follows the methodology proposed in [33].

In surveillance applications, being able to detect and localize a target at a given time is not always sufficient for granting the necessary level of situational awareness, especially in the maritime domain. As a matter of fact, it is typically required also to provide an estimate of the trajectories of all the detected targets in a monitored area. Therefore, it is essential to extract as much information as possible about the target "state space model" (e.g., its position and speed) from the set of available noisy detections (i.e., target detections and false alarms), which are described by the sensor "measurement model" [35]. This problem can be divided into the "data association" and "track update" steps. In this paper, the first step consists in the application of the so-called joint probabilistic data association (JPDA) rule. This rule, in combination with the second step represented Kalman filter (KF) tracking strategy, provides an effective solution to the multiple target tracking (MTT) problem, with a good trade-off between performance and complexity [35]. However, the target classification problem goes well beyond the scope of this paper and it will be thoroughly addressed in future works.

III. Simulation Scenario Modeling and Results

The proposed MIMO radar system must operate in a real maritime scenario, which is more complicated and demanding than the one already considered for a first validation [12], [13], [14]. Therefore, the mission requirements make more complex

TABLE I
RPs WGS-84 Coordinates and Antennas Pointing Directions

	RP$_1$	**RP$_2$**	**RP$_3$**
Longitude	10°17'29.6'' E	10°17'50.1'' E	10°17'45.3'' E
Latitude	43°33'30.1'' N	43°33'11.2'' N	43°32'57.3'' N
Dir. vs North	185°	225°	265°

the system design due to many variables, like the MIMO system RPs number and the network topology, the required probability of detection P_D, conditioned by the set false alarm probability P_{FA}, the required spatial resolution necessary for target classification purposes, and so on. These can be translated into operational requirements and hardware parameters, after a proper system analysis carried out to find the best trade-off between system performance and complexity. Here, we report the simulations that demonstrate that, once set the system requirements, it is possible to attain the needed performance, thanks to the added value of spatial and frequency diversities provided by the multi-band coherent MIMO radar with widely distributed antennas. Then, from those requirements, the system design parameters are derived.

A. The MIMO system model

Coherent RF signal distribution using photonics enables the concept of a coherent MIMO radar network with largely distributed sensors. Indeed, photonics inherently guarantees the required coherence and high-capacity links [9], [15]. Preliminary experiments and simulations on photonics-enabled largely distributed, coherent, multi-band MIMO radar systems, have been recently demonstrated, and the results confirm the potential of these systems [14], [31], [36].

The system design steps from some relevant parameters of the real scenario. To survey the port internal area, the maximum targeted range for each RP can be set around 2 km. Each RP is equipped with one S-band and one X-band horn antenna. At these operational frequencies, which are typically employed for airborne and maritime surveillance applications, compact antennas provide a good gain and are easily deployable. Moreover, by fixing the minimum detectable RCS of an isotropically scattering target to 3 dBsm (2 m^2), we have considered the system working in a sort of worst case, targeted to optimize the system surveillance capability also in case of low-RCS highly maneuvering targets, which could represent a threat for navigation, or head towards a sensitive infrastructure. These assumptions mean that, by accepting a system noise figure (NF) of 10 dB, a minimum detectable signal (MDS) as low as -110 dBm, the necessary signal-to-clutter-plus-noise ratio (SCNR) in the covered area must be >11.7 dB for the S band (i.e., at 2.9 GHz), and >6.5 dB for the X band (i.e., at 9.7 GHz), as respectively depicted by the blue and red curves in Fig. 3 a). Here, we adopt the CA-CFAR detection scheme analyzed in [33], considering a nominal P_{FA} of 10^{-4}, which is a common value for surveillance radar systems. Fig. 3 b) shows that, employing 3 RPs deployed in the positions sketched in Fig. 1, whose exact coordinates are reported in Table I, the achieved SNCR is increased up to 25 dB, guaranteeing a continuous coverage of the area of interest with a P_D close to 1, as reported in Fig. 3 c) and almost perpendicular observation capability between RP_1 and RP_3.The RF signal bandwidth has been also selected considering other requirements, as explained in the following.

Employing 3 RPs, the MIMO radar network we present here is composed by a total of four nodes, considering also the CU, as sketched in Fig. 1 and Fig. 4 a). With respect to the already demonstrated down-scaled architecture [12], [13], [14], it has an additional RP, and two working bands instead of one. In total, it relies on 18 virtual channels. This choice represents the best minimum configuration allowing the system to exploit enough virtual channels for granting the adequate level of target detection and localization capabilities, without dramatically increasing the architectural complexity. From Fig. 4 a), the CU includes the system master optical clock. The electrical radar waveform is synthesized at intermediate frequency (IF) and undergoes electro-optical (E/O) conversion before being distributed over single mode fiber (SMF) to the RPs, where the opto-electric (O/E) conversion operates the signal upconversion from IF to RF frequency (see Sect. V). Each RP can upconvert the radar waveform up to both S and X band, with an appropriate RF front-end for each band, including a high-power amplifier (HPA) that boosts the signal before transmission by the antenna. The radar echoes back-scattered from the targets are gathered again by the antennas, amplified on each band by a low-noise amplifier (LNA), and E/O-converted, to be sent back to the CU over a SMF link. Once in the CU, the received echoes are O/E-converted, realizing their downconversion at IF, and digitized before processing. The proposed system exploits time-division multiplexing (TDM), meaning that when a RP transmits the S-band signal, the others keep silent; then, all the RPs receive. Then, the same RP transmits the X-band signal, and the scheme repeats. Afterwards, another RP transmits while the others receive, and so on, in a round-robin fashion.

The signal processing approach employed in the port scenario is sketched in Fig. 4 b). Once the signals from all the virtual channels are acquired and digitized, non-coherent MIMO processing is carried out for monitoring the possible presence of targets over a large area. The CFAR algorithm is used to detect them, and, only in a second moment, coherent MIMO processing is applied to image targets in the cells where detections have occurred. Finally, from the set of available detections, the number of targets and their tracks (i.e., trajectories) can be estimated. Thus, the same radar system may

TABLE II
SYSTEM MAIN DESIGN PARAMETERS

Parameter	Value/Description
No. of TXs x RXs	3 x 3
Single RPs max range	2 km
Signal Waveform	Linear Freq. Mod. (LFM) Chirp
X-band Carrier Frequency	9.7 GHz
S-band Carrier Frequency	2.9 GHz
Intermediate Frequency	100 MHz
Pulse duration	100 ns to 5 μs
Chirp Bandwidth	100 MHz
Pulse Repetition Interval (PRI)	50 μs
Output Power per antenna	10 W (40 dBm)
Sampling Frequency	400 MHz
Horn Antenna Gain/Aperture	25 dBi/≈20°
Overall System NF	10 dB
Minimum Detectable Signal	-110 dBm
Coherent Integration Gain	43 dB

be able to provide the command & control platform (see Sect. V.A) and the system operator with information at different levels of refinement, such as target detection, tracking, classification, identification, and even behavior assessment if artificial intelligence (AI) techniques are used.

Finally, it is worth mentioning that a thoughtful analysis of these techniques, as well as their optimization, goes beyond the scope of the present work, which is meant to describe the main system design steps of a photonics-assisted MIMO radar in the field of maritime surveillance.

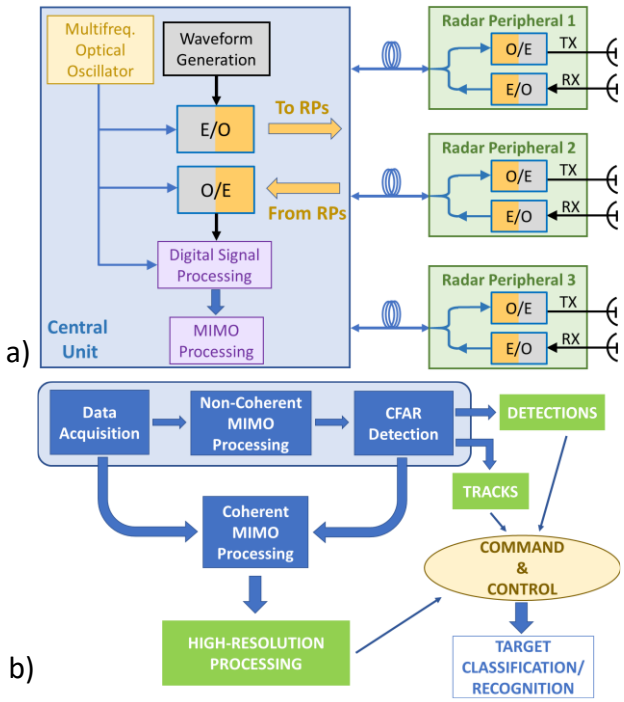

Fig. 4. Block diagram representing a) the architecture of the CU+3RPs and b) the prospective processing chain of a surveillance photonics-assisted MIMO radar system. E/O: Electro-optical conversion; O/E: Opto-electric conversion.

B. Target Detection and Imaging Capabilities

The translation of mission requirements into system metrics, as summarized in Sect. III, has evidenced how the system parameters and its configuration shown in Fig. 2, have been optimized based on performance metrics related to detection probability in revealing simple point-like targets. Then, after this optimization, it is necessary to assess the system performance, in terms of target detection, tracking capabilities, and classification potential when close-to-reality scenarios are considered, e.g., in case of multiple extended targets.

For this reason, we simulate the system operation in a typical situation that ports are often called to manage, consisting in the monitoring of the entry maneuvers performed by a large cargo vessel ($L_{cargo} = 150$ m), which is towed by a tugboat ($L_{tugboat} = 32$ m), and escorted by a small pilot boat ($L_{pilot} = 8$ m). The positions of the targets have been extrapolated from a real AIS data record, and the three targets proceed towards North-East. In the considered configuration, the farthest target end is located at around $d_{max} = 1.3$ km from RP_1, the center of the local ENU coordinate system. Fig. 5 shows the processing outputs for a surveilled square area having 400 m side. To speed-up processing operations and limit the demand of computational resources, initially a rough search for targets is performed with non-coherent processing, dividing the monitored space into a grid of 4×4 m^2 pixels, roughly corresponding to twice the monostatic range resolution granted by the radar waveform (i.e., ~1.5 m for 100 MHz signal bandwidth). To make an initial comparison between the performance of classic monostatic radars and a MIMO system, the 2D ambiguity functions, normalized with respect to the maximum value, are calculated for the stand-alone RP_1, RP_2 and RP_3, as shown in Fig. 5 a), 5 b) and 5 c), respectively. Intuitively, the color-coded plots depict the likelihood of the target presence in the monitored area, where the dark-blue color indicates a low probability of target presence, while the yellow color denotes a very high probability. As expected, with only one RP sensor working at a time, it is possible to provide only range (or range-Doppler) information about the targets, with 1.5-m range resolution, and a very rough cross-range resolution increasing with the target distance, attaining ~454 m at d_{max}. Moreover, no 2D spatial information can be extracted by the monostatic patterns. Apparently, the situation remains almost unvaried when the CU contemporaneously drives two RPs, as shown in Fig. 5 d), e), and f), respectively for the RP_1-RP_2, RP_1-RP_3 and RP_2-RP_3 pairs. Again, it is very difficult to extract useful information about the targets, especially the tugboat and cargo. Only in the case of Fig. 5 d), it is possible to reveal the presence of the cargo bridge located at the stern.

Finally, when the signals coming from all the three RPs are fused together, as in the case of the non-coherent MIMO ambiguity function shown in Fig. 5 g), it is possible to visually reveal the presence of all the three targets and to intuitively understand which ship parts are characterized by high scattering properties (e.g., bow, stern, bridge, wheelhouse, tower cranes). As a matter of fact, CFAR detection, which is performed on the non-coherent MIMO ambiguity function shown in Fig. 5 g), permits to numerically reveal the presence of the pilot boat and tugboat and of the main structures of the cargo ship close to the bow and stern, as shown in Fig. 5 h). Here, the range-gating method described in [33] is considered, for mitigating the number of false alarms. As we can observe, the areas subtended by target detections are almost all within the vessel shapes described by the red contours.

These promising results suggest that it could be even possible to estimate the size of the targets, and to do some further inference on their main structures, for classification and recognition purposes. For this reason, the coherent MIMO ambiguity function has been calculated over the same grid area, with the output depicted in Fig. 5 i). The chosen 4×4 m^2 pixel resolution format does not allow to accurately pinpoint at the main target structures in the 2D map. For this reason, the coherent MIMO processing can show superior performance if the amplitudes of the ambiguity functions around the three targets are evaluated with finer grids. To reduce computational complexity and time, the coherent processing is performed over smaller regions of interest (ROIs), centered around the target centroids. These ROIs are sufficiently large to include each

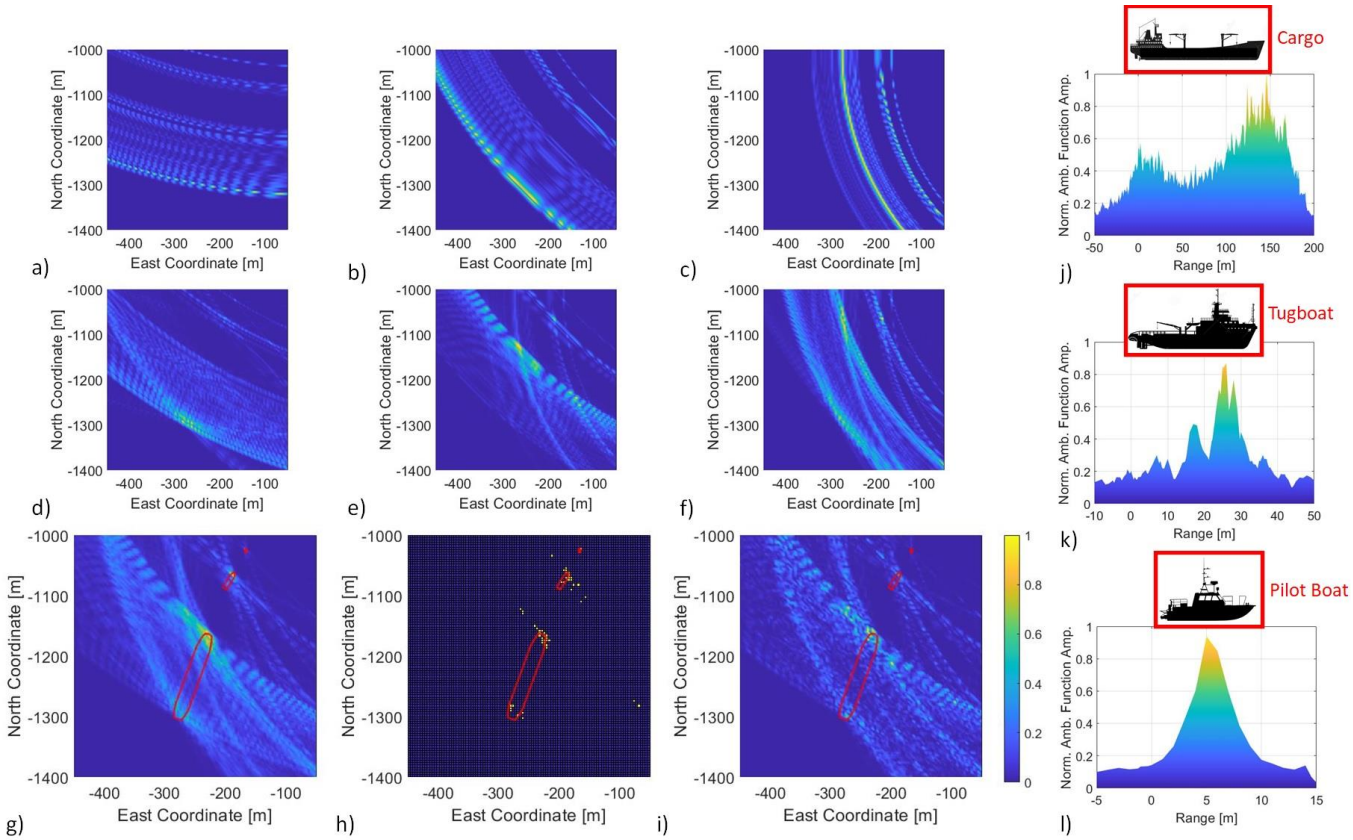

Fig. 5. Typical port surveillance scenario: a large cargo ship enters the port, escorted by a pilot boat, and towed by a tugboat. The three targets proceed towards North-East. Their silhouettes are depicted by red contours; a, b, c): 2D ambiguity functions calculated at RP_1, RP_2 and RP_3, respectively; d, e, f) non-coherent 2D ambiguity functions calculated for the RP_1-RP_2, RP_1-RP_3 and RP_2-RP_3 2x2 system configurations, respectively; g) non-coherent 2D ambiguity function calculated for the 3x3 system configuration; h) CFAR detection evaluated from the non-coherent MIMO ambiguity function; i) coherent 2D ambiguity function calculated for the 3x3 system configuration; amplitude of the dual-band coherent MIMO ambiguity functions calculated for the 3x3 system configuration: j) cargo ship, k) tugboat, and l) pilot boat.

target, and they can be described by a grid of 1×1 m^2 pixels. The results of such analysis, displayed in range-amplitude plots, are shown in Fig. 5 j), k), and l) for the cargo ship, tugboat, and pilot boat, respectively. Although obtained from simulations, the peaks of the ambiguity functions closely follow the main vessel structures, such as the prominent bow and stern of the cargo vessel, as well as the first tower crane, see Fig. 5 j). Similar comments can be done for the coherent outputs referring to the tugboat and pilot boat, for which it is possible to extract the positions of the wheelhouse and mainmast, see Fig. 5 k) and l). These results suggest that it could be possible, given the right processing methodology, to classify the detected target. Further research in this sense is currently ongoing.

IV. The Photonics-Assisted Multi-Band MIMO Radar Implementation

The simulation reported in the previous section confirm the system suitability to a real freight port scenario, showing the potential target detection and imaging capability, obtained with the set minimum RCS detectability requirements, along with the P_{FA} and P_D. These requirements have been translated into hardware design parameters, which are reported in Table II and employed for the implementation of the CU and the RPs.

The detailed system architecture is depicted in Fig. 6, with details of the CU structure in Fig. 6 a). The master optical oscillator is implemented by a mode-locked laser (MLL) with repetition frequency f_r = 400 MHz, whose comb-like spectrum, sketched in Fig. 6 c), inset A, is split by an arrayed-waveguide grating (AWG). Thus, the lines, spanning over more than 550 GHz (i.e., 4.5 nm), are separated in groups in the frequency (or wavelength) domain at the AWG output ports. In this way, the pulsed laser spectrum is sliced in sub-combs, whose width is Δf_{AWG} = 50 GHz (i.e. 0.4 nm), composed by ~125 f_r-spaced lines. Two spectrum slices are allocated to every RP, a first one for the TX, a second for the RX. To avoid any crosstalk, the related AWG output ports are not adjacent, so that the two sub-combs for the same RP are 100-GHz apart. The first sub-comb enters an electro-optical modulator (EOM) and is modulated by the radar waveform at f_{IF} = 100 MHz, operating the E/O conversion. The signal is a linear frequency-modulated (LFM) pulse, whose bandwidth and duration can vary. The obtained spectrum, as in point B of Fig. 6 a), is sketched in Fig. 6 c), inset B. The second, unmodulated sub-comb is depicted in Fig. 6 c) inset C; it is coupled with the modulated one, along with a gate signal generated by directly modulating a distributed feed-back (DFB) laser. The latter is employed for the remote control of the RPs. Then, the obtained optical signal is boosted by an Erbium-doped fiber amplifier (EDFA) and transmitted to one specific RP. Fig. 6 c), inset D, represent the overall optical signal after amplification (point D in Fig. 6 a). For each RP, a parallel, identical system branch performs the very same

This article has been accepted for publication in IEEE Journal of Selected Topics in Quantum Electronics. This is the author's version which has not been fully edited and content may change prior to final publication. Citation information: DOI 10.1109/JSTQE.2021.3092880

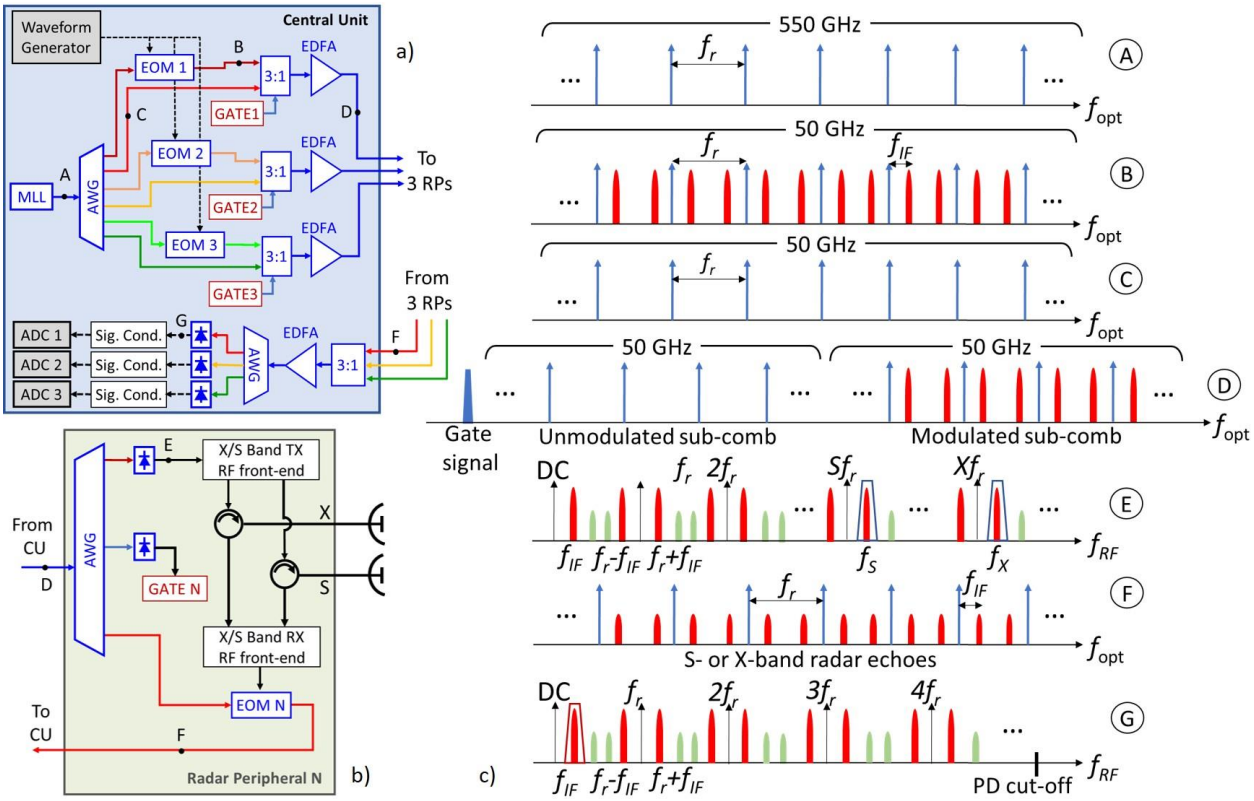

Fig. 6. 3x3 TX/RX MIMO radar system detailed architecture; a) Central Unit architecture; b) Radar Peripheral architecture; c) Spectra of the involved optical signals as they propagate in the CU and in the RP. The circled letters labelling the insets correspond to the sketch of the optical spectrum at the point marked with the same letter on the CU or RP architectures. EOM: Electro-optical; AWG: Arrayed-waveguide; EDFA: Erbium-doped fiber amplifier; ADC: analogue-to-digital converter; MLL: Mode-locked laser; Sig. Cond.: Signal conditioning; RP: Radar peripheral; CU: Central unit; DC: Direct current; PD: Photodetector.

operations, although on a different set of optical frequencies. Fig. 7 reports pictures of the implemented CU (a) and RPs (b). Fig. 7 c), on the other hand, depicts the optical spectra of the MLL (grey curve), and the of the AWG outputs in the CU, separating the unmodulated (blue, orange, green curves at lower wavelengths) and modulated sub-combs (blue, orange, green curves at higher wavelengths). A different color is associated to each RP.

At the RP (see scheme in Fig. 6 b), the optical received signal is the same as in point D, except the attenuation due to the SMF link. Its components are again separated by an AWG, and the modulated sub-comb is heterodyned in a photodetector (PD), giving rise to the spectrum in point E of Fig. 6 c), represented in Fig. 6 c), inset E. The PD output is composed by many beat products. To obtain the frequency upconversion, only the ones centered at frequencies f_S = 2.9 GHz and f_X = 9.7 GHz are selected for transmission, as highlighted in Fig. 6 c), inset E. Considering that $f_S = Sf_r + f_{IF}$ and $f_X = Xf_r + f_{IF}$, we can obtain the desired carrier frequencies by setting S = 7 and X = 24. Afterwards, the S- and X-band waveforms are separated onto two front-end branches, amplified by the HPAs and transmitted by the antennas (one for the S, one for the X band).

The back-scattered radar echoes are received and, after amplification by the LNA and filtering, they are E/O-converted by modulating the second received unmodulated optical sub-comb (see Fig. 6 b). At the EOM output (point F), an optical spectrum like the one sketched in Fig. 6 c), inset F, is obtained. The signal is then delivered to the CU thanks to SMF links. This operation is carried out by all the three RPs, and the three optical signals collected at the CU are coupled, amplified by a single EDFA, separated again by an AWG on three parallel channels, and O/E-converted to obtain downconversion to IF by narrow-band PDs. At the PDs output, the beat product at the lowest frequency is selected, as it is highlighted in the corresponding spectrum reported in Fig. 6 c), inset G. Then, the signals are amplified to match the amplitude range of the ADCs, digitized, and processed. To test the capability of the system to guarantee the needed sensitivity, Fig. 7 d) reports the extinction ratio calculated between the AF main lobe and the highest sample of the noise floor, showing that each single RP can detect a MDS of -110 dBm. Better performance is shown in the X-band, because of a less noisy front-end.

Since all the employed optical signals are originated from the same MLL, they are phase-locked to each other. This is a feature that ensures the high level of coherence of the employed signals. Moreover, optical distribution does not degrade the signals stability, and coherence is maintained all over the entire networks. To quantitively assess the impact of signal distribution on coherence, the studies conducted in [12], [14] have evaluated the effect of a 10 km SMF link, which revealed to be negligible in the short period, but highlighting a slight drift of < 5° over multiple hours, mainly due to thermal fluctuations. These results, reported in Fig. 7 e), are below the maximum tolerated phase drift for performing coherent MIMO processing, estimated to around 6° [37]. Finally, Fig. 7 f) and

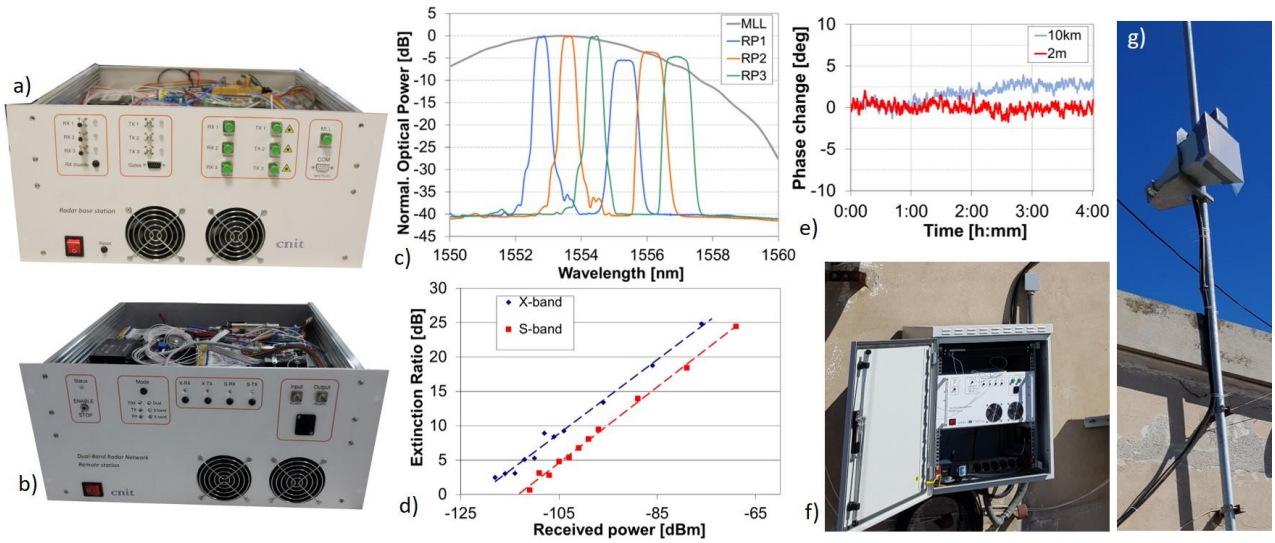

Fig. 7. The implemented MIMO system: a) The CU, or base station; b) One RP, or remote station; c) Normalized optical spectra exiting the CU: the sub-combs are represented in blue, orange, green (the right-most group of three: modulated sub-combs; left-most ones: corresponding unmodulated subcombs), whereas the grey line sketches the MLL overall original spectrum; d) Phase stability analysis over time of the distributed optical signals; e) RPs extinction ratio of the AF peak to the noise floor for in S and X band, as a function of the received power; f) One installed RP with g) its X- and S-band antennas.

g) depict an installed RP, with its S- and X-band antennas.

The architecture of a MIMO radar may pose scalability challenges, depending on the particular selected implementation. Photonics-assisted systems, as the one we describe here, do not represent big scalability problems in terms of numbers of employed RPs. Each RP needs two optical frequency sub-combs (in this case, portions of the MLL spectrum employed as a master oscillator) for E/O and O/E conversion of the IF and RF signals. The optical sub-combs frequency span must be large enough to ensure that all the targeted RF carriers can be generated. The higher the RF carriers, the larger the needed sub-comb span; subsequently, the overall optical comb spectrum must be large enough. To make an example, in our case, the 550 GHz span of the MLL spectrum would enable employing up to 15 RPs emitting signals at frequencies up to the K_u band. However, larger optical combs can be easily obtained from MLLs or thanks to non-linear effects in optical resonators [38], allowing for a larger number of RPs. Furthermore, in the presented implementation, the limited number of RPs allows for a TDM approach, in which transmission is done in a round robin-fashion. This way, with *N* RPs, *N* PRIs will be needed for the transmission by all the RPs. If *N* is large, time needed to illuminate the target from all the viewpoints is long, contributing to increase the decorrelation between the virtual channels. This can be avoided by employing a set of orthogonal waveforms that can be simultaneously transmitted by all RPs is a single PRI, paying some additional system complexity as a price for scalability. Yet, it is necessary to understand if the performance of a MIMO radar indefinitely increases increasing the number of virtual channels: should the performance show an upper bound, it could be worth pursuing a trade-off between performance and scalability. This matter is still under investigation.

V. Sensor Output Information Integration

In maritime surveillance systems, it may be desirable to integrate AIS navigation reports with data acquired by radar systems and networks, for improving the reliability (in terms of performance, temporal, and spatial coverage) of the maritime situational awareness (MSA) picture. The joint use of radar and AIS data, allows to discriminate between cooperative and non-cooperative targets and to provide information about possible threats, navigational risks, to optimize resource allocation capabilities for greater efficiency, safety, and cost savings.

In this context, MIMO radars are sought for providing early-warning detection and supplementary coverage for detecting targets too small for carrying an AIS transponder. For this reason, the proposed photonics-assisted MIMO radar has been conceived for being integrated with the MoniCA platform, operating in the Livorno Port. This section introduces MoniCA focusing on the integration of the MIMO radar within MoniCA.

A. The MoniCA Standard Platform

MoniCA Standard Platform is a service-oriented architecture for agile microservices development and data lake management addressing shipping and navigation, distributed monitoring, eFreight, logistics and corridors, eMobility, data reporting. The adoption of a standard and service-oriented approach enables the integration of existing systems into a single flexible and interoperable architecture. Furthermore, the adoption of new architectural elements, such as data virtualization layer (DVL) and cloud components allow to define more efficient process control policies (service and user management, security, data access, etc.) preserving the scalability of the whole system.

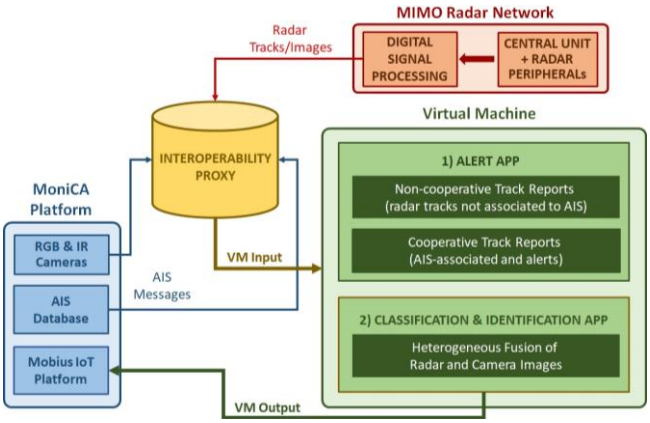

Fig. 8. Scheme of the interaction between the photonics-assisted MIMO radar network and MoniCA.

The MoniCA architecture [18] consists of different decoupled layers, such as the Infrastructure as a Service (IaaS) consisting of physical components, like the surveillance MIMO radar network, the SMF backbone, the 5G/Wi-Fi mesh network, distributed IoT sensors like monitoring cameras, weather, and acoustic stations; Platform as a Service (PaaS) for data lake management performing data collection, processing, aggregation; Software as a Service (SaaS), as an environment for microservices management. As shown in the yellow block in Fig. 8, MoniCA is equipped with:

a) Two red-green-blue (RGB) video and infrared (IR) surveillance cameras;
b) A database, which sends AIS navigation data, queried by the Interoperability Proxy (IP);
c) The Mobius IoT platform, which stores the information (i.e., the AIS-associated and alert tracks) processed by the virtual machine (VM).

B. Integration of the photonic MIMO radar with MoniCA

The interaction workflow between the proposed photonics-assisted MIMO radar and the MoniCA standard platform is depicted in Fig. 8, where it is ideally divided into "process" blocks running at every new data push. It starts with the remote acquisition of raw data operated by the MIMO RPs, and the CU hands its output (i.e., target trajectories and images) to the IP, which manages the data streams from the different platforms. Then, the IP pushes radar data to the VM, which collects the estimated target tracks and associates them with the AIS data stream, for distinguishing between cooperative and non-cooperative targets (i.e., "Alert App"). The IP then recasts the information to MoniCA IoT platform Mobius using the oneM2M standard. At this point, MoniCA can also activate a 45x zoom of cameras on a specific target of interest, which are jointly processed with the radar images obtained from coherent MIMO processing. Non-cooperative tracks can be, thus, further processed through the "Classification & Identification App" for providing the support operator a more complete MSA picture.

To test the communications between the radar system and MoniCA platform, the same scenario described in Sect. IV.C has been considered, in which the radar signals collected by the RPs are simulated from real AIS records in the MoniCA database. At every new radar data acquisition and processing step, the currently available target tracks, obtained according to the procedure described in Section II.D, are forwarded to MoniCA to a dedicated container via hypertext transfer protocol (HTTP) messages. These messages, containing the dynamic (e.g., position and velocity) and static (e.g., estimated length and width) information about all the target tracks recorded at a specific time, are parsed into a JavaScript object notation (JSON) string and then formatted in such a way that are compliant to the oneM2M standard. Data just created are sent to the platform using the representational state transfer (REST) protocol which notifies to the dashboard server the presence of new radar readings. Finally, these information are displayed on the MoniCA dashboard. The dashboard is developed using Node.js (back-end side) and hypertext markup language (HTML), cascading style sheets (CSS) and JavaScript frameworks (front-end side).

A sample representation of the principle of functioning of the MoniCA dashboard when the photonics-assisted MIMO radar is operated is given in Fig. 9. In the chosen time interval, most of the monitored vessels remain "at anchor" inside the port around the internal wharves, while two very clear target trajectories (i.e., fuchsia and cyan) head outside of the port area, following the ferry navigation routes. The dashboard is conceived such that a new color is associated to any new incoming track, and the operator can select specific tracks by clicking on their color-coded markers, to visualize both present and historical information about the target of interest. This information can be enriched by the possibility of visualizing the surveilled area and the targets thanks to the RGB/IR cameras, simply clicking on the green squares.

VI. CONCLUSION

Microwave photonics has made feasible the extension of the concept of network to the radar world, also enabling MIMO radar systems to fully exploit the information extracted from the collected data, thanks to centralized processing. Executing processing of raw data in a single CU implies, in principle, no loss of information in the data fusion, and this is possible thanks to the inherent coherence granted by photonics in signal generation, up- and down-conversion, and distribution.

Following the outdoor validation of a first MIMO radar functional model, in this paper we report on the advances in the deployment of a MIMO radar system in a real operational maritime scenario. Starting from the mission requirements, an analysis based on simulations has been carried out to design the

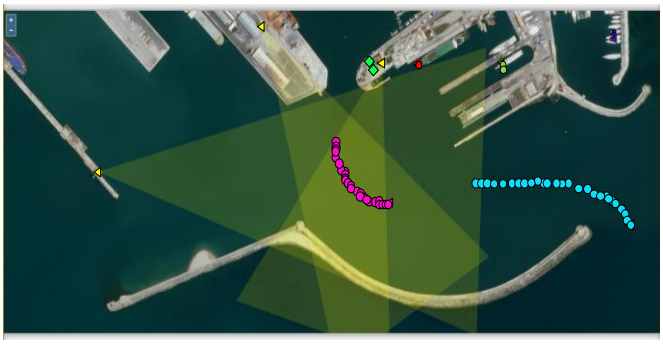

Fig. 9. Principle of functioning of the MoniCA dashboard when the photonics-assisted MIMO radar is operated. Radar peripherals are represented by the solid yellow triangles; areas illuminated by the RPs are depicted by the transparent yellow triangles; RGB/IR cameras are depicted by the solid green square; target trajectories are depicted by the color-coded dots.

system hardware architecture and to optimize the processing. The translation of the requirements into architectural parameters aimed also at the best trade-off between performance, in terms of detection probability, resolution, target localization and imaging accuracy, and complexity, above all in terms of number and distribution of RPs.

The advantages of the proposed 3 TX x 3 RX, dual-band MIMO architecture with respect to stand-alone, monostatic radars have been confirmed, by simulating the detection of multiple targets with different size. Both non-coherent and coherent MIMO processing is performed, transmitting S- and X-band waveforms. The system shows enhanced capabilities of target accurate localization and classification, notwithstanding the presence of a very large target that usually can mask the presence of smaller objects. Moreover, the possibility of the MIMO radar to cooperate with the port monitoring platform is shown. The MIMO system can indeed hand over its data to the VM merging the outputs coming from many sensors and data sources, contributing to the enhancement of the MSA and to an efficient implementation of the Port of the Future paradigm.

ACKNOWLEDGMENT

The Authors would like to thank Eng. I. Toni, D. Del Giovane, Dr. A. Querci of the Port Network Authority of the North Tyrrhenian Sea and Capt. S. Maggiani of the Livorno Port Pilots, for the fruitful collaboration and the possibility of deploying and testing the MIMO radar network in the port.

REFERENCES

[1] M. Hermann, T. Pentek, B. Otto, "Design Principles for Industrie 4.0 Scenarios," *2016 49th Hawaii International Conference on System Sciences (HICSS)*, Koloa, HI, 2016, pp. 3928-3937.

[2] UNCTAD (2020d*). Review of Maritime Transport 2020*. United Nations publication. Sales no. E.20.II.D.31.

[3] Ch. Mason, "Ports Must Be Smarter to Thrive in the Future", *Port Technology International*, 2019-09-18 (Retrieved 2021-02-16).

[4] L. Cavalli, G. Lizzi, "Port of the Future. Addressing efficiency and sustainability at the Port of Livorno with 5G," Ericsson, GFTL-20:000714 Uen, June 2020.

[5] A.J. Seeds, K.J. Williams, "Microwave Photonics," *IEEE J. Lightwave Technol.* n. 24, vol. 12, pp. 4628-4641 (2006).

[6] G. Serafino, *et al.*, "Microwave Photonics for Remote Sensing: From Basic Concepts to High-Level Functionalities," *IEEE J. of Lightwave Technol.*, vol. 38, no. 19, pp. 5339-5355, Oct. 2020.

[7] D. Marpaung, J. Yao, J. Capmany, "Integrated Microwave Photonics," *Nature Photon.* 13, pp. 80–90 (2019).

[8] F. Zhang, B. Gao, S. Pan, "Photonics-based MIMO radar with high-resolution and fast detection capability," *Opt. Expr.*, 26 (13), pp. 17529-17540 (2018).

[9] G. Serafino, *et al.*, "Towards a New Generation of Radar Systems Based on Microwave Photonic Technologies", *IEEE J. Lightw. Tech., vol.* 37, no. 2, pp. 643-650, 2019.

[10] G. Serafino, *et al.*, "Photonic approach for on-board and ground radars in automotive applications", *IET Rad., Son. & Nav.* 12 (10), 1179-1186, 2018.

[11] F. Laghezza *et al.*, "Field evaluation of a photonics-based radar system in a maritime environment compared to a reference commercial sensor," *IET Radar, Son. & Nav.*, vol. 9, no. 8, pp. 1040–1046, 2015.

[12] F. Scotti, *et al.*, "Widely Distributed Photonics-Based Dual-Band MIMO Radar for Harbour Surveillance," *IEEE Photonics Technology Letters*, vol. 32, no. 17, pp. 1081-1084, Sept. 2020.

[13] S. Maresca, *et al.*, "Photonics for Coherent MIMO Radar: an Experimental Multi-Target Surveillance Scenario," *2019 20th International Radar Symposium (IRS)*, Ulm, Germany, 2019, pp. 1-6.

[14] S. Maresca, *et al.*,"Coherent MIMO radar network enabled by photonics with unprecedented resolution," *Opt. Lett.* 45 (14), pp. 3953-3956 (2020).

[15] P.A.Williams, W.C. Swann, N.R. Newbury, "High-stability transfer of an optical frequency over long fiber-optic links," *J. Opt. Soc. Amer. B*, vol. 25, no. 8, pp. 1284–1293, 2008.

[16] J. Fu, S. Pan, "A fiber-distributed bistatic ultra-wideband radar based on optical time division multiplexing," *Intern. Top. Meet. Microw. Phot.*, 2015, pp. 1–4.

[17] https://safety4sea.com/cm-moby-prince-italys-worst-maritime-disaster-since-world-war-ii/. (Retrieved 2021-06-17).

[18] P. Pagano *et al.*, "Complex Infrastructures: The Benefit of ITS Services in Seaports" in *Intelligent Transportation Systems: from Good Practices to Standards*, Taylor & Francis Group, Boca Raton (USA), 2020.

[19] V.S. Chernyak, *Fundamentals of Multisite Radar System*, Gordon & Breach Science Publ., London (1998).

[20] A.M. Haimovich, *et al.*, "MIMO radar with widely separated antennas", *IEEE Signal Processing Magazine*, vol. 25, no. 1, pp. 116-129 (2008).

[21] H. Godrich, *et al.*, "Target Localization Accuracy Gain in MIMO Radar-Based Systems", *IEEE Trans. on Inf. Theory*, vol. 56, no. 6, June 2010.

[22] D.W. O'Hagan, S.R. Doughty, M.R. Inggs, *Chapter 5 - Multistatic radar systems*, pp. 253-275, in "*Academic Press Library in Signal Processing, Volume 7: Array, Radar and Communications Engineering*", Ed. R. Chellappa and S. Theodoridis, Elsevier, 2018.

[23] N.H. Lehmann *et al.*, "MIMO-radar application to moving target detection in homogeneous clutter," *Adaptive Sensor Array Proc. Workshop at MIT Lincoln Laboratory*, Waltham, MA, July 2006.

[24] S. Alhuwaimel, *et al.*, "First measurements with NeXtRAD, a polarimetric X/L Band radar network," *2017 IEEE Radar Conference (RadarConf)*, Seattle, WA, 2017, pp. 1663-1668.

[25] M.R. Inggs *et al.*, "Report on the 2018 Trials of the Multistatic NeXtRAD Dual Band Polarimetric Radar," *2019 IEEE Radar Conference (RadarConf)*, Boston, MA, USA, 2019, pp. 1-6.

[26] M. Akcakaya, *et al.*, "MIMO Radar Detection Under Phase Synchronization Errors," in *Proc. of the 2010 IEEE Int. Conf. on Acoustics, Speech and Signal Processing (ICASSP)*, Dallas, TX, pp. 2578-2581, 2010.

[27] T.E. Derham, S.R. Doughty, K. Woodbridge, C. J. Baker, "Design and evaluation of a low-cost multistatic netted radar system," *Radar, Sonar and Navigation*, IET, vol. 1, no. 5, pp. 362–368 (2007).

[28] M. Inggs, H. Griffiths, F. Fioranelli, M. Ritchie, K. Woodbridge, "Multistatic radar: System requirements and experimental validation," *2014 International Radar Conference*, pp. 1-6, Lille, France (2014).

[29] F. Santi, F. Pieralice, D. Pastina, "Joint Detection and Localization of Vessels at Sea With a GNSS-Based Multistatic Radar," *IEEE Trans. on Geoscience and Remote Sensing* 57 (8), pp. 5894-5913 (2019).

[30] R. Bil, M. Brandfass, J.P. van Bezouwen, "Future Technological Challenges for High Performance Radars," *19th International Radar Symposium* (IRS), pp. 1-10, Bonn, Germany (2018).

[31] P. Ghelfi, F. Laghezza, F. Scotti, D. Onori, A. Bogoni, "Photonics for Radars Operating on Multiple Coherent Bands," *IEEE J. of Lightwave Technol.*, vol. 34, no. 2, pp. 500-507, Jan. 2016.

[32] F. E. Nathanson, *Radar Design Principles*, McGraw-Hill, 1969.

[33] S. Maresca, A. Bogoni, P. Ghelfi, "CFAR Detection applied to MIMO Radar in a Simulated Maritime Surveillance Scenario," *2019 16th Europ. Radar Conf. (EuRAD)*, Paris, France, 2019, pp. 157-160.

[34] N. Janatian, *et al.*, "CFAR Detectors for MIMO Radars," *Circuits, Systems and Signal Processing*, vol. 32, pp. 1389-1418, 2013.

[35] Y. Bar-Shalom, *et al. Tracking and Data Fusion: A Handbook of Algorithms*, YBS Publishing, Storrs, CT, USA, (2011).

[36] L. Lembo, P. Ghelfi, A. Bogoni, "Analysis of a Coherent Distributed MIMO Photonics-Based Radar Network," *2018 15th European Radar Conference (EuRAD)*, Madrid, pp. 170-173, 2018.

[37] I. Pasya, and T. Kobayashi, "Detection performance of M-sequence-based MIMO radar systems considering phase jitter effects," *2013 IEEE Int. Symp. on Phased Array Sys. and Tech.*, Waltham, MA, USA, pp. 394-398.

[38] A.L. Gaeta, M. Lipson, T.J. Kippenberg, "Photonic-chip-based frequency combs" *Nature Photon*. 13, 158–169 (2019).

Giovanni Serafino is assistant professor at the, Sant'Anna School of Advanced Studies of Pisa, Italy, from which he received *cum laude* the Ph.D. in Emerging Digital Technologies in 2013. Among his past and actual research interests, there are

all-optical signal processing, fiber-optic transmission systems, reconfigurable nodes for optical networks, applications of microwave photonics techniques to radar systems and wireless communications, including optical beamforming for 5G and photonics-assisted coherent MIMO radars. He is coauthor of more than 20 papers on international journals and more than 60 papers on conference proceedings, two book chapters, and five patents.

Salvatore Maresca received the M.S. degree in Telecommunications Engineering and the Ph.D. degree in Information Engineering from the University of Pisa, Italy, in 2006 and 2010, respectively. In July 2010, he joined the NATO Centre for Maritime Research and Experimentation (CMRE), La Spezia, Italy. In 2016 he joined the CNIT, Pisa. Since January 2018, he is Senior Researcher at the TeCIP Institute of Sant'Anna School of Advanced Studies, Pisa. His research activity is in statistical signal processing of radar data, with a special focus on sea clutter analysis, target detection and tracking strategies, data and information fusion in MIMO radars. He has authored and coauthored more than 35 scientific and technical publications and reports, and two book chapters.

Luca Di Mauro received his B.D. in computer science in 2016 from University of Pisa. He joined the Networks of Embedded Systems area at CNIT as a vehicular communications and IoT researcher working in the AUTOPILOT project in 2017. He worked as a researcher in Scuola Superiore Sant'Anna in Pisa to develop applications for road safety of vulnerable users in a smart city environment. His research interests have a specific focus on C-ITS systems, wireless sensors networks, and embedded systems.

Alexandr Tardo received his M.S. degree in Telecommunications Engineering in 2015 from University of Catania. In 2015, he has conducted industrial research related to ICT technologies and advanced applications for control, monitoring and management of processes as well as systems for risk prevention at University of Catania. In 2016, he has been involved in research and development activity related to Interoperability Platform for Health Cloud at Telecom Italia. In 2017, he joined CNIT, working on supply chain digitalization not only at the Port of Livorno. From 2018 he leads R&D activities, including the usage of cutting-edge technologies as well as service-oriented architectures in seaports, coordinating and managing relevant technical boards as well as EU projects.

Antonio Cuillo is a CNIT affiliated and a former Port Network Authority of the North Tyrrenian – Innovation Department Member. He received a Post-Degree Master in Logistics from Pisa University. He worked in the system integration with MoniCA Standard Platform especially for what concerns the IoT framework. He also oversaw the development of the user dashboards of some MoniCA prototypal services, like weather monitoring and noise emission monitoring.

Filippo Scotti received the M.Sc. degree in physics engineering from the Politecnico di Milano, Italy, in 2009. In 2009, he was with the PGT-Photonics, Milan, Italy, for a six-month internship. Since 2010, he has been a researcher with CNIT, Pisa, Italy. He has authored or coauthored more than 60 papers in international journals and conferences, holding five patents. His research interests include microwave photonics for radar and sensing applications and fiber optic transmissions with particular interest in all-optical signal processing.

Paolo Ghelfi received the M.Sc. degree in Electronic Engineering, in 2000. Since 2001, he has been with the PNT Laboratory CNIT, Pisa, Italy, where he is currently the Head of Research Area. His current research focuses on microwave photonics, with strong experience also in the fields of high bit rate fiber-optic transmission systems, all-optical signal processing, and reconfigurable networks. He has authored or coauthored more than 40 papers on international journals, more than 110 papers on international conferences, more than 20 patents, and two book chapters.

Paolo Pagano received his Ph.D. degree in High Energy Physics from Trieste University, having worked for the COMPASS collaboration at CERN. He holds a Master in IT from Scuola Superiore Sant'Anna in Pisa. From October 2015 he is the director of the joint CNIT / Port Network Authority of the Northern Tyrrhenian Sea laboratory on advanced sensing and networking in seaports. His research activities have a specific focus on ITS and Port of the Future. He is participating to the ETSI standardization committees for Cooperative ITS and maritime communication (ETSI ISG CDM). He co-authored about 100 peer reviewed papers in international journals and conferences.

Antonella Bogoni is a Professor of Sant'Anna School of Advanced Studies of Pisa, and Director of the PNT Laboratory of CNIT, Pisa, Italy. Her research interests include photonics technologies for optical fiber networks for ultrafast optical signal processing and microwave systems, especially for 5G, radars, and space applications. Moreover, she is leading the design of specific photonic integrated circuits for implementing on-chip the proposed solutions. She authored and coauthored 56 patents, 8 books and chapters, and more than 160 papers on the main scientific international journals (22 invited contributions). She has more than 300 contributions in the main photonics and radar international conferences, winning 9 best paper awards, with more than 50 invited contributions. She is the Topical Editor for Optics Letters and part of the reviewers Board of Wiley Ed., Nature Photonics, IEEE/OSA journals. She is Chair of conferences and workshops, including Program Chair of ECOC 2018, Subcommittee Chair of ECOC 2015, and General Chair of Photonics in Switching 2014.